Reprinted from SPIE Vol. 209—Optical Signal Processing for C3I

Optical processors for adaptive phased-array radar

David Casasent, Demetri Psaltis, B. V. K. Vijaha Kumar, Mark Carlotto
Department of Electrical Engineering, Carnegie-Mellon University
Schenley Park, Pittsburgh, Pennsylvania 15213

Abstract

A coherent optical correlator (operating on the heterodyned received signals from a phased array and a non-coherent iterative vector-matrix electro-optical processor (operating on the covariance matrix of received array signals) are described as candidate advanced processors for adaptive phased array radar.

1. Introduction

The processing requirements of adaptive phased array radars [1-4] require advanced signal processing techniques and architectures with real-time and parallel processing capacity and with the ability to accommodate a large number of adaptive array elements. Optical signal processors appear to be quite appropriate for this problem. In this paper we describe the design, analysis and initial experiments performed on two such optical processors for adaptive phased array radar.

2. Adaptive phased array radar signal processing

A phased array radar system can be described most simply by considering the 1-D phased array radar (transmitting or receiving) system shown in Fig. 1. Beam steering in such systems is achieved by varying the weights W_n applied to each element n of the array. If the same weight is applied to all elements, the beam is steered on-axis or at boresight. The resultant beam pattern is described by

$$E(\theta) = K \frac{\sin[(\pi nd/\lambda)\sin\theta]}{\sin[(\pi d/\lambda)\sin\theta]} \quad , \tag{1}$$

where d is the spacing between each of the N phased array elements. The pattern described by Eq. (1) is the classic sinc x = [sin (x)]/x pattern. If the phases ϕ_n of the weights W_n applied across the array elements increase linearly across the array, the resultant beam pattern from the array will be steered to $\theta = \theta_o$ where θ_o is proportional to the phase gradient across the array. The array has higher gain in the direction of the beam than it has at all other directions. These other directions constitute the sidelobes of the array pattern. When properly designed the radar will respond to signals backscattered from targets located within the directed beam while being relatively insensitive to objects and other signal sources within the sidelobes. This enables the classification of received energy as signals or noise depending on whether it is present in the main beam or in the sidelobes respectively. When the noise energy is much higher than the signal energy, the radar system becomes unable to discern the target and performance is deteriorated. However, if the sidelobe response can be altered in the direction of such noise sources, system performance can be recovered. In order to alter the array factor to this end, it is necessary to augment the phase and/or amplitude weight of each element so that the pattern has maximum gain in the direction of the steered beam and minimum response in the sidelobe region corresponding to noise sources.

In an adaptive phased array, the weights at each element are chosen to place nulls at the angular locations of interfering noise power incident at the antenna. This provides a great increase in detectable SNR. The adaptive weights W_n vary with time and are functions of the time-varying external noise field. To determine W_n, the expected values or time averages of the products of all pairs of signals V_i and V_j received at array elements i and j are determined. The co-variance matrix M with components

$$M_{ij} = \int V_i(t) V_j^*(t)\, dt$$

is then formed. The weights $\vec{W}$ in vector notation are related to the co-variance matrix M and the steering vector $\vec{S}$ by

$$\vec{MW} = \vec{S}^* \tag{2}$$

The desired weights $\vec{W}$ for the N array elements can then be obtained from $\vec{S}^*$ and the inverse M^{-1} of the covariance matrix as described by

$$\vec{W} = M^{-1}\vec{S}^* . \tag{3}$$

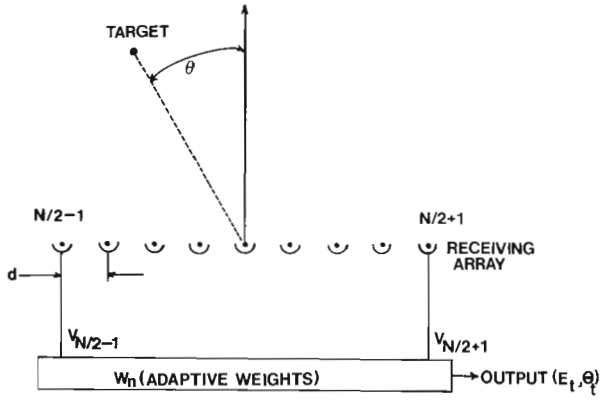

Fig. 1 Phased array radar receiving scenario and notation.

The weights are usually found by solving (3) given M. The major computational load associated with such an approach is the matrix inversion. For large arrays, the dimensions of M are large and its inversion requires considerable computation time and large memory storage requirements. In Section 3, we describe a coherent optical multichannel correlator (COC) that operates on the received signals at N array elements to produce an output that is a map of the angular noise field's distribution $N_m(\theta_m)$, where θ_m is the angle of noise source m and N_m is its strength. The inverse DFT of the output of the COC system yields the desired weights. In Section 4, we describe a non-coherent electro-optical iterative optical processor (IOP) that solves (2) using the algorithm

$$\vec{W}_{i+1} = \vec{S}^* + (I-M)\vec{W}_i, \tag{4}$$

where I is the identity matrix and $\vec{W}_i$ is the estimate of the adaptive weights after iteration i. When $\vec{W}_i = \vec{W}_{i+1}$, the system's output $\vec{W}$ is the solution to (2).

3. Coherent optical correlator system

3.1 System

The COC system used is shown in Fig. 2. It is a multichannel version of the conventional optical frequency plane correlator [5] with special purpose post electronics. For an N element array with M noise sources of strengths N_m and located at angles θ_m, we describe the received signal at array elements n due to noise source m as $f_{nm}(t-\tau_{mn})$, where

$$\tau_{mn} = k\,(R-n)d\,\text{Cos}\,\Theta_m,$$

$k = 2\pi/\lambda$ and the reference array element R is the central one.

The signal received at elements n and R are thus

$$f_n(t) = \sum_m^M f_{Rm}(t-\tau_{mn})$$

$$f_R(t) = \sum_m^M f_{Rm}(t).$$

In the system of Fig. 2, a multichannel matched filter with transmittance $F_R^* = \mathcal{F}^*[f_R]$ is placed at P_2 and the received signals f_n are recorded on N lines at P_1. At P_2, Lens L_1 forms the 1-D FT of the P_1 pattern. Leaving line n at P_2, we find $F_n\,F_R$.* Lens L_2 forms the 1-D FT of the light distribution leaving P_2 and at line n at P_3 we find $f_n \circledast f_R$.

3.2 Analysis

We described the P_3 pattern at line n as

$$f_R \circledast f_n = \sum_m^M \sum_j^M [f_{Rm}(t) \circledast f_{Rj}(t-\tau_{jn}) \tag{5a}$$

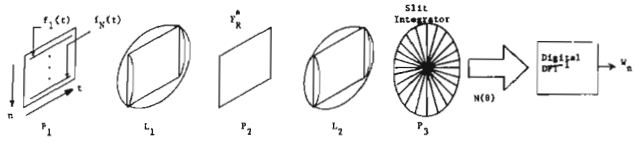

Fig. 2 Schematic diagram of the COC processor for adaptive phased array radar.

$$f_R \circledast f_n = \sum_m^M [f_{Rm}(t) \circledast f_{Rm}(t-\tau_{mn})] \tag{5b}$$

$$= \sum_m^M C_m(t-\tau_{mn}), \tag{5c}$$

$$= \sum_m^M N_m \delta(t-\tau_{mn}), \tag{5d}$$

where (5b) results when the noise sources are independent and (5d) follows if the power of the m-th noise source is N_m and its spectrum is white in which case $C_m(t) = N_m\delta(t)$.

3.3 Slit Integration

For a single noise source m, the P_3 output will consist of N correlation peaks, one on each of the N output channels with delays

$$\tau_{mn} = K_n \cos\theta_m,$$

where n denotes the channel number and the variable m corresponds to different noise source angles θm and different angles in the output correlation plane. Thus, for each noise source, τ_{mn} is linearly related to n with a slope that is related to the angle θm of the m-th noise source. Thus, to determine $N_m(\theta m)$, we integrate the P_3 pattern along diagonal slits. The outputs from M such slit integrations of the entire P_3 pattern from (5) is

$$I_m = \sum_n^N f_R(t) \circledast f_n(t)\delta(t-\tau_{mn})$$

$$= \sum_n^N Nm = N \cdot N_m, \tag{6}$$

or N times the power of the m-th noise source.

3.4 Experimental Data

In Fig. 3, we show the P_3 output pattern due to two bandpass stochastic noise sources at angles $\theta m = \pm 5^o$ and strength $N_1 = 2N_2$. In Fig. 4, we show $N_m(\theta m)$ obtained by slit integration (using, for example, slit-shaped detector elements). As expected, the $N(\theta)$ output in Fig. 4 exhibits peaks at $\pm 5^o$ that differ by 3dB.

3.5 Statistical Analysis

The statistical nature of the noise source and its effect on the accuracy of the $N(\theta)$ output has also been considered. As a measure of system performance, we chose SNR defined as the magnitude squared of the estimated value of the noise at the correct location divided by its variance far from registration. Assuming a correlation model of the form $R_s(\tau) = \exp(-a|\tau|)$, where "a" is a measure of the signal's bandwidth, we obtain for large "at" time bandwidth SNR = NaT. From this, we find that SNR and hence the accuracy of the estimate of θ_m increases as N, bandwidth or the signal's observation time T increases.

A similar analysis of the system's resolution was conducted using two sources at $\pm\beta_1$ with two sources defined as resolvable if $I(\beta_1)/I(0) \geq 2$. A statistical analysis showed the equivalent resolvability condition to be $R(\beta_1)/R(0) \geq KN$, where K is a constant of order 1/8 and R is the ensemble autocorrelation function for each noise source. This analysis showed that resolution improves as N increases as expected, but moreso that it was independent of observation time T_a.

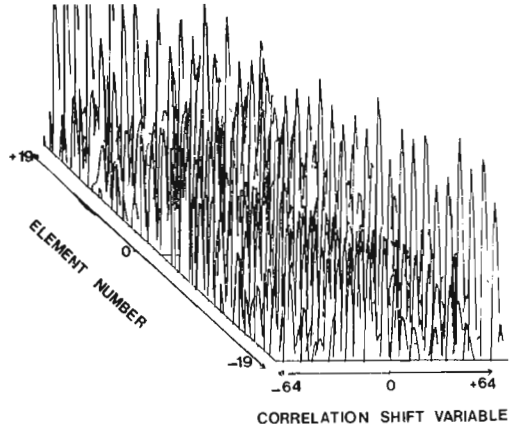

Fig. 3 Output plane pattern at P_3 of Fig. 2 for two bandpass noise sources at $\pm 5^{\circ}$, one with twice the strength of the other.

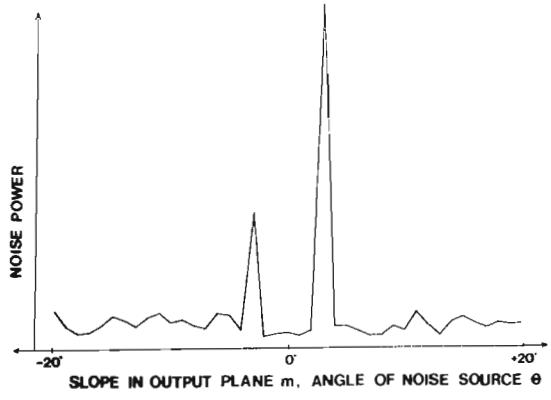

Fig. 4 COC Output of Fig. 3 after slit integration to yield angular noise field distribution $N_m(\theta_m)$.

An analysis [6] in which the covariance matrix M is computed, inverted and $\vec{W}$ computed as in (3), has shown that 2NB seconds of data (or 2N samples, where B is the bandwidth of the noise source) are needed per antenna element for the SNR of the far field pattern to be within 3dB of the optimum (assuming M were known completely).

3.6 Post Processing

We next considered the post-processing required to compute $\vec{W}$ from $N_m(\theta m)$. As showed in Fig. 2, a simple inverse DFT is the most desirable post-processing. Two measures were used to determine the weights. When SNR was maximized, we found $\vec{W} = KC^{-1}U$, where K = constant, U = unit column vector, and C has elements C_{ij} as in (5). Thus, all C_{ij} pairs must be computed to obtain $\vec{W}$ to maximize SNR. The second measure chosen was to minimize noise. In this case, $\vec{W} = C_1^{-1}U$, where C_1 is a modified matrix and thus only one column of the inverse matrix need be computed. This latter approach is far simpler and allows direct use of the COC output.

For a linear array with uniform element spacings d and for a single frequency noise source, we found that the weights W_n can be obtained from θm as

$$\sum_n W_n \exp(-j2\pi kn) = \exp(j2\pi bk), \tag{7}$$

where $b = 2\pi\nu d(\cos\theta)/\lambda$. From (7), we see that W_n can be found from the inverse DFT of the right-hand side of (7), which in turn is the output of the COC after slit integration.

4. Iterative optical processor

4.1 System

The IOP system is shown in Fig. 5. The input plane contains N LEDs with outputs An, that are imaged vertically and expanded vertically onto a mask at P_2 with transmittance b_{nm}. Leaving the n-th row at P_2, the light distribution is

$$a_n b_{n1} + \ldots + a_n b_{nM}. \tag{8}$$

The output from P_2 is imaged horizontally and focused vertically onto a linear detector array at P_3, where the vector-matrix product $\vec{A}B$ results [7].

To use this system for adaptive radar processing [10], the transmittance of the mask at P_2 is made proportional to [I-M] and S*is added to the detector's output, which is fed back to the LEDs at P_1. If we denote the LEDs output at one iteration by W_i, the system realizes (4). When $W_i = W_{i+1}$, the output W is the solution (3) to the adaptive radar equation (2).

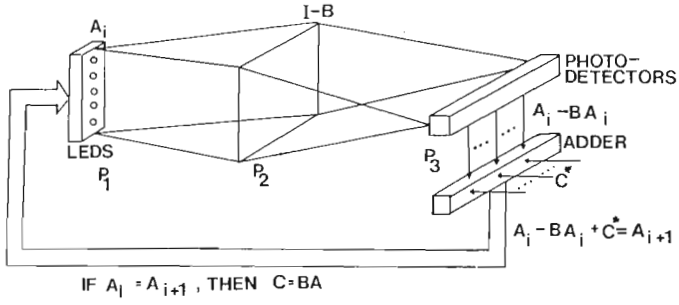

Fig. 5 Schematic diagram of the IOP processor for adaptive phased array radar.

4.2 Complex Data

Complex data can be processed in this iterative system by representing each complex quantity by its components along the axes at 0°, 120°, and 240° in complex space [8] or by other methods such as color multiplexing [9]. By properly arranging the elements of the P_2 mask, complex vector-matrix multiplications are possible on this system.

4.3 Experimental Data

To demonstrate the use of this processor for adaptive radar, 6 input LEDs were used with a 6X6 element mask at P_2 to model the complex signals from a 2 element adaptive radar with an 0.1 watt noise source at $\theta = 60^{\circ}$ and receiver noise of 0.5 watts. The 6 photodiode outputs at the 1st, 2nd and 5th iteration are shown in Fig. 6. They agree well with the predicted results.

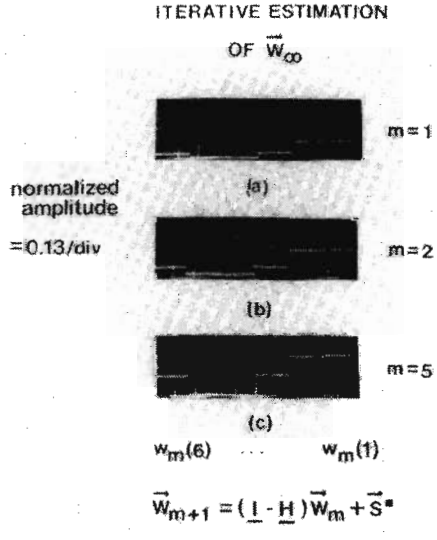

Fig. 6 Outputs from the six photodiode detector elements in the IOP after iterations 0, 1, and 5. Comparisons to theoretical data shows the excellent agreement and accuracy of this IOP system.

4.4 Advanced System

The system presently under fabrication is shown schematically in Fig. 7. This system uses 20 input LEDs, fiber optic connections are used between P_1 and P_2 and the detector at P_3 is mounted flush against the P_2 mask. Addition of S* is achieved by an extra row of the P_2 mask. Complex data can be handled using another row of the mask for bias purposes. Pulse-width modulation of the LED source array outputs and time integration at the detector output is used to improve the system's accuracy. Correction for various component errors is performed by a ROM in the electronic feedback circuit, with the entire system under a microcontroller. System iteration times below 1 usec are possible with this system.

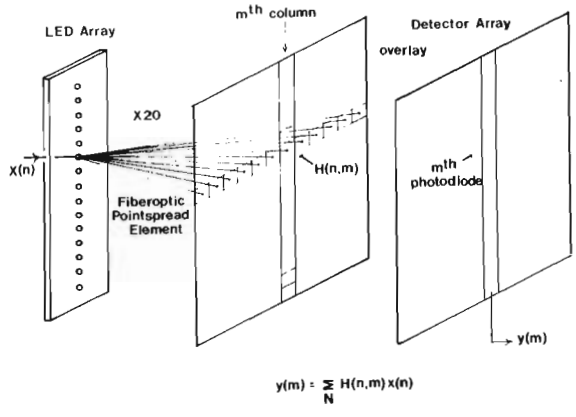

Fig. 7 Schematic diagram of advanced IOP system with fiber optic connections.

Acknowledgments

This research was supported by Contract F-30602-78-C-0272 from Rome Air Development Center. The authors thank RADC for support of this research and especially our Contract Monitor, V. Vannicola, for his constant direction and guidance throughout this program.

References

[1] B. Widrow, et al., Proc. IEEE, 55, 2143 (1967).

[2] S. Appelbaum, Syracuse Univ. Res. Corp., Rept. SPO-TR-tt-1 (August 1966).

[3] I.S. Reed, J. D. Mallett and L. E. Brennan, IEEE, AES-10 (November 1974)

[4] V. Vannicola, SPIE, 209 (1979).

[5] A. Vander Lugt, IEEE, IT-10, 139 (1964).

[6] W. Liles et al., Multidomain Algorithm Evaluation, RADC-TR-78-59, TSC, April 1978.

[7] J. W. Goodman, A. R. Dias, and L. M. Woody, Opt. Letts., 2, 1 (1978).

[8] J. W. Goodman and L. M. Woody, Appl. Opt., 16, 2611 (1977).

[9] D. Psaltis et al., Opt. Lett., (November 1979).

[10] D. Psaltis et al., SPIE, 180 (1979).